THE JOURNAL OF PHYSICAL CHEMISTRY A

Article

pubs.acs.org/JPCA

Modeling the Interaction of Nanoparticles with Mineral Surfaces: Adsorbed C_{60} on Pyrophyllite

Runliang Zhu,[†,‡] Marco Molinari,[‡] Thomas V. Shapley,[‡] and Stephen C. Parker*[,‡]

[†]Guangzhou Institute of Geochemistry, Chinese Academy of Sciences, Guangzhou 510640, China

[‡]Department of Chemistry, University of Bath, Claverton Down, Bath BA2 7AY, United Kingdom

ABSTRACT: We have applied DFT and molecular modeling to investigate the interaction between carbon-based nanoparticles (CNPs) and geosorbents using the adsorption of buckminsterfullerene (C_{60}) on pyrophyllite and comparing it to the aggregation of C_{60} molecules. The approach is transferable and can be readily applied to more complex CNP−clay systems. We predict that C_{60} molecules adsorb preferably on the mineral surface and that the most stable adsorption site is the ditrigonal cavity of the surface. The free energy of adsorption on pyrophyllite was calculated to be more favorable than aggregation both in a vacuum (−0.47 vs −0.41 eV) and in water (−0.25 vs −0.19 eV). In aqueous environments, there are energy barriers as the C_{60} molecule approaches either a surface or another C_{60} molecule, and these occur upon disruption of the hydration layers that surround each component. There are also free energy minima that correspond to outer-sphere and more favorable inner-sphere complexes. We expect this adsorptive behavior to be a general feature of CNP−clay systems, and as clays are ubiquitous in the environment, it will offer an inexpensive remediative method to prevent the widespread impact of molecular C_{60} and CNPs.

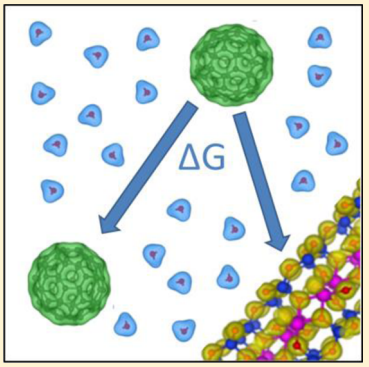

1. INTRODUCTION

Carbon-based nanomaterials have received increasing interest because of their unique physicochemical properties and potential applications in various fields.[1,2] Buckminsterfullerene (C_{60}) represents one of the most important carbon-based nanoparticles (CNPs), and its industrial-scale production has reached the level of tons.[3] Because C_{60} has been suggested to be toxic to organisms, although this toxicity is still debated as it might depend on synthesis methods and solvents,[4,5] the potential adverse effects of C_{60} on human health and the environment require serious attention, as most C_{60} will eventually end up in the environment.[4−7] Indeed, the aqueous aggregation of C_{60} and its interactions with various geosorbents have been suggested to play a critical role in its environmental fate and transport and, hence, have received much research interest.[8−11] C_{60} has an extremely low aqueous solubility (7.96 ng/L), and beyond that concentration level, it forms nanosized aggregates (nC_{60}).[12,13] Therefore, most previous experiments concerning the toxicity and transport of this CNP focused on nC_{60} rather than molecular C_{60}.[4,5,8,11] However, because of its smaller size, molecular C_{60} will be less easily trapped by porous natural media than nC_{60} and is more readily transported in water, which suggests that molecular C_{60} controls the environmental distribution, leading to a wider environmental impact. However, because the aqueous solubility of C_{60} is beyond the detection limits of most instruments, the interactions between molecular C_{60} and geosorbents have not yet been well explored. Although Chen and Jafvert[8] estimated the distribution coefficient of molecular C_{60} between soil organic carbon and water from the distribution coefficients between soils and mixtures of water and ethanol, this is a very challenging process, and hence, new ways of achieving these distribution coefficients are required.

Recent molecular dynamics (MD) simulations have shown computer modeling to be a powerful approach for studying the hydration and aggregation of C_{60} in water.[14−22] This approach has the advantage of providing atomic-level insight into the effect of microstructures on material properties by evaluating both kinetic and thermodynamic data.[14,15] Several MD studies have calculated the structure of the water surrounding C_{60} molecules, the hydration energy of C_{60}, and the aggregation free energy of C_{60} molecules.[14−22] In general, they suggest that the strong dispersion interactions between C_{60} and water lead to stable hydration shells around C_{60} because of the high carbon density and that this results in a water-induced repulsion between hydrated C_{60} molecules.[14,15,18,19] Experimentally, Labille et al. studied the dispersion of C_{60} in water, confirming the presence of adsorbed molecular water as well as adsorbed hydroxyl groups. However, no evidence of how molecular water is oriented on the C_{60} surface has been reported.[13]

Little is known about how the efficiency of clay surfaces as geosorbents compares with the aggregation of solutes. Clay minerals are an important class of materials and are widely used in composites, paints, drilling liquids, cosmetics, and medicines. Hence, they have been the subject of many previous computational studies; see, for example, the works by Cygan et al.[23] and Heinz,[24] which discuss both quantum and classical methods. Indeed, a number of classical atomistic models have

Received: March 22, 2013
Revised: June 12, 2013
Published: July 1, 2013

been successfully developed for clay minerals in the past few decades, such as those of Boek et al.[25] and Skipper et al.,[26] along with the widely used CLAYFF[27] and PFF.[24,28]

As computer power continues to develop, simulation techniques are increasingly used to supplement experimental data with complementary information.[29] In the present study, we investigate the adsorption of C_{60} on a clay mineral and compare this adsorption to the aggregation of C_{60} molecules. Because the surfaces of many clay minerals are primarily composed of siloxane,[30] the pyrophyllite (001) surface without substitution or a net charge was selected as representative of a clay mineral surface. Pyrophyllite, $Al_4[Si_8O_{20}](OH)_4$, is a smectite clay mineral with the simplest composition of the 2:1 dioctahedral phyllosilicates (Figure 1a). It is a layered material composed of slabs arranged perpendicular to the c direction, in which octahedrally coordinated aluminum atoms linked by hydroxyl groups are sandwiched between two sheets of SiO_4 tetrahedra.[31] The distance between adjacent slabs is termed the interlayer spacing. The slabs, called TOT layers, are held together by van der Waals interactions, and hence, the (001) surface of pyrophyllite is a perfect cleavage plane, as shown in Figure 1c. In contrast to other minerals that require rebonding and hydroxylation,[32−35] the (001) surface of clay does not need any saturation of the dangling bonds, causing the surface compositions in dry and wet environments to be the same. Indeed, Lindgreen et al. showed this to be the surface topology in water, albeit for illite, a more complex smectite, using atomic force microscopy (AFM).[37] The surface stability and the affinity of clay minerals including pyrophyllite for water are discussed in more detail by Heinz[24] and Sposito et al.[36] and references therein.

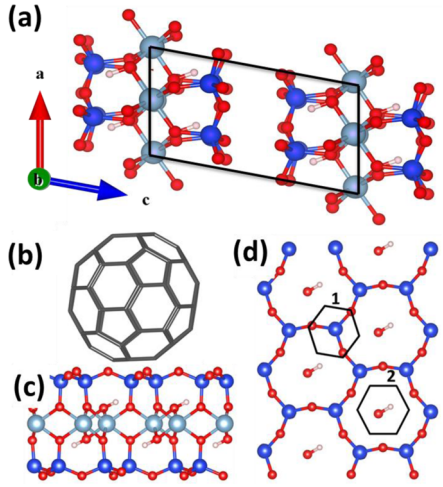

Figure 1. (a) Bulk pyrophyllite, (b) C_{60} molecule, (c) side view of the pyrophyllite surface, (d) top views of the C_{60} molecule 6-ring on (1) a surface silicon atom and (2) the ditrigonal cavity of the surface. C, gray; O, red; Si, blue; Al, light blue; H, white.

In the present article, we show that atomic-level modeling can be used to gain insight into the general problem of how to model the interactions of nanoparticles with mineral surfaces. After describing the details of the simulations in section 2, we discuss our results in section 3 and present our conclusions in section 4.

2. METHODOLOGY

Density functional theory (DFT) and potential-based molecular dynamics were applied to calculate the properties of bulk pyrophillite (Figure 1a), the adsorption energy of C_{60} (Figure 1b) on pyrophyllite (Figure 1c), the energy of aggregation of two C_{60} molecules, and the interaction energy between molecular C_{60} and water. Potential of mean force (PMF) calculations were then used to evaluate the free energy profiles for both the adsorption and aggregation processes.

2.1. DFT Calculations. DFT calculations were performed using the VASP code,[38,39] in which a plane-wave basis set describes the valence electronic states and the projector augmented wave (PAW) approach[40,41] models the core−valence interaction. The exchange and correlation were treated by the generalized gradient approximation (GGA) using the Perdew−Burke−Ernzerhof (PBE) functional.[42] The inability of electronic structure methods to account for van der Waals interactions is well-known.[43,44] A number of different methods that apply dispersion corrections to DFT methodologies are available, as discussed by Dobson et al.[43] In this work, we employed the DFT-D2 method of Grimme,[45] which applies dispersion corrections in a pairwise manner, and the vdW-DF method of Klimeš et al. based on the optB86b exchange functional[46] as implemented in the VASP code. Three-dimensional boundary conditions were used throughout. Bulk pyrophillite consiting of stacked TOT layers (Figure 1a) was modeled using a $6 \times 4 \times 2$ Monkhorst−Pack k-point mesh and a plane-wave cutoff of 500 eV to ensure convergence. To check the stability of the bulk over a single slab, we performed simulations doubling the unit cell along the c direction and removing the middle TOT layer with a $6 \times 4 \times 1$ k-point mesh. The (001) surface employed for the adsorption study was modeled using the slab method[47] in which a single layer of pyrophyllite (15.58×18.03 Å^2 containing six $Al_4[Si_8O_{20}](OH)_4$ formula units; Figure 1c) was used to generate two identical surfaces through the introduction of a 30 Å vacuum gap of perpendicular to the surface to minimize the interaction between images. Given the use of a large supercell in the calculations (240 atoms and 1152 electrons) and the insulating nature of the material, it was considered adequate to use the Γ point for k-point sampling. All calculations were spin polarized, and relaxation of the atomic structure for all atoms was deemed to have converged when the forces were less than 0.01 eV Å^{-1}.

The adsorption energy of molecular C_{60} was modeled by comparing the sum of the energies of the optimized molecule and clay slab separately with the energy of C_{60} added to one side of the slab. A dipolar correction was included along the axis perpendicular to the surface for all surface calculations to remove any error in the electrostatic energy due to the periodicity perpendicular to the surface. For investigations of the aggregation of two C_{60} molecules, two configurations were considered, in which the two molecules interacted through the 5- or 6-rings. For the interaction between C_{60} and H_2O, the water molecule was placed on top of a 5- or 6-ring, with and without the hydrogen atoms pointing toward the C_{60} surface.

As noted earlier, all configurations were also minimized with the inclusion of the van der Waals interaction energy.

2.2. MD Simulations. MD simulations were performed using the DL_POLY_2 code,[48] which employs standard force fields (FFs) in which the forces between ions consist of a long-range Coulomb term and a short-range potential. The

dx.doi.org/10.1021/jp402835v | J. Phys. Chem. A 2013, 117, 6602−6611

electrostatic interactions were evaluated using the Ewald method to a precision of 10^{-5}. The short-range force cutoff was set to 10 Å for all simulations. The equations of motion were updated using the Verlet-leapfrog algorithm. We used the canonical (*NVT*) ensemble with a time step of 1 fs. The temperature was kept constant by means of a Nosé–Hoover thermostat.

We primarily used CLAYFF to represent pyrophyllite and the flexible SPC model for the water solvent,[27] although as discussed in section 3.4, we tested the sensitivity of the results to the details of the potential by using another successful clay potential, PFF,[28] which is fully compatible with CVFF.[55] In general, these force fields have been successfully employed for modeling various clay minerals and water.[49−54] Different force fields were tested for C_{60}. We compared CVFF,[55] Dreiding,[56] and Amber,[57] calculating the adsorption energy of C_{60} on pyrophyllite and the aggregation energy of two C_{60} molecules in a vacuum, with ab initio results. A pyrophyllite slab containing 18 unit cells ($3 \times 6 \times 1$) was used with a simulation cell of approximately $21 \times 36 \times 100$ Å^3 ($a \times b \times c$) and with a vacuum gap in the c direction. The adsorption process for C_{60} on pyrophyllite was investigated both in a vacuum and in water. When the solvent was included, 1200 water molecules were added to the C_{60}–pyrophyllite system, forming a layer approximately 50 Å thick. Calculations were run at 300 K for 2 ns. Data from the last nanosecond was used to analyze the properties of the system.

PMF calculations were employed to calculate the free energy of adsorption of C_{60} on the pyrophyllite surface and the free energy of aggregation of two C_{60} molecules both in a vacuum and in water. First, the center of mass of C_{60} was constrained at 80 incremental positions moving away from the surface by approximately 0.2 Å. At each position, a 1 ns MD simulation was run. The free energy of adsorption was then obtained by integrating the average force needed to constrain the molecule at a specific position as a function of distance.[58,59]

3. RESULTS AND DISCUSSION

We start by presenting a comparison of the lattice parameters for the pyrophyllite crystal structure and the cleavage and interaction energies between the different components of the system [water, C_{60}, and the (001) surface of pyrophyllite] (section 3.1). The use of reliable electronic structure simulations allowed us to assess the performance of the force fields. We then used the most appropriate model to first evaluate the structure of the mineral–water interface and the diffusion of the C_{60} molecule on the pyrophyllite surface (section 3.2). Second, the calculations of the free energy associated with the adsorption of C_{60} onto pyrophyllite and the aggregation of two C_{60} molecules are discussed in section 3.3. Finally, section 3.4 concludes the results by presenting a comparison between PMF calculations on the adsorption of C_{60} onto pyrophyllite evaluated using two of the clay force fields.

3.1. DFT versus Force Fields. Table 1 presents a comparison between the geometry-optimized bulk lattice parameters for bulk pyrophyllite obtained using DFT and the two force fields CLAYFF and PFF. Potential-based calculations were performed using the METADISE code.[60] Both models were found to represent the experimental results with a good degree of accuracy. The overestimation of the c parameter from unmodified DFT is due to the lack of inclusion of the vdW interactions that are responsible for holding the TOT layers together. A further means of assessing the reliability of the two techniques is to evaluate the cleavage energy of bulk pyrophyllite due to the stacking of TOT layers compared to the energy of a single TOT layer. DFT, DFT-D2, vdW-DF, and CLAYFF gave values of 0.01, 0.23, 0.31, and 0.15 J m^{-2} per unit $Al_4[Si_8O_{20}](OH)_4$. All values were positive, indicating the stability of the bulk compared to the single TOT layer. However, it is evident that unmodified DFT does not capture the full extent of the interaction between the TOT layers.

Table 1. Lattice Parameters Calculated from Energy Minimization Using DFT with and without the Inclusion of vdW Interactions, CLAYFF, and PFF

	a (Å)	b (Å)	c (Å)	α (deg)	β (deg)	γ (deg)
DFT	5.22	9.07	9.98	91.91	100.20	89.71
DFT-D2	5.17	9.00	9.35	91.11	100.89	89.80
vdW-DF	5.17	8.98	9.30	90.92	100.92	89.86
CLAYFF	5.18	9.02	9.29	90.43	98.31	89.51
PFF	5.18	8.97	9.28	90.61	101.10	90.12
expt[a]	5.160	8.966	9.347	91.18	100.46	89.64

[a]Experimental data from ref 31.

The quality of the net interactions within the clay–water–C_{60} system was assessed by comparing the interaction energies and final geometries of van der Waals corrected DFT and several force fields.

We identified the equilibrium configurations by placing the C_{60} molecule in a range of different orientations and performing geometry optimization. Figure 1d shows the two most stable adsorption sites found: C_{60} adsorbed through the 6-ring and through the 5-ring. Table 2 lists the lowest energy values of adsorption/aggregation for the different methods. The first three rows give the DFT results. The results in the first row do not include a van der Waals correction, whereas results employing two different approaches for including vdW are presented in rows 2 and 3. It is clear that the standard DFT approach gives incorrect results and clearly demonstrates the need for the inclusion of vdW dispersion interactions. The calculated interaction energies of a C_{60} molecule adsorbed through either its 5- or 6-ring show negligible differences. The preferred adsorption site, site 2 in Figure 1d, for molecular C_{60} is the ditrigonal cavity of pyrophyllite and is more stable than site 1 by only 0.07 eV. Aggregation of C_{60} molecules is marginally more energetically favorable when they approach each other through the 5-rings; however, the largest energy difference is only 0.04 eV. The average distances of carbon atoms in different molecules are 3.4 and 3.6 Å depending on

Table 2. Interaction Energies (eV) within the System Pyrophyllite–H_2O–C_{60} Calculated Using DFT with and without the Inclusion of vdW Interactions and Different Force Fields[a]

	C_{60}–pyro	C_{60}–C_{60}	C_{60}–H_2O	H_2O–pyro
DFT	0.03	0.08	0.10	−0.06
DFT-D2	−0.65	−0.50	−0.10	−0.20
vdW-DF	−0.84	−0.36	−0.07	−0.19
CLAYFF (Amber)	−0.50	−0.26	−0.04	−0.21[b]
CLAYFF (CVFF)	−0.86	−0.74	−0.07	
CLAYFF (Dreiding)	−0.65	−0.45	−0.05	
PFF	−0.61[c]		−0.08	−0.16

[a]In all cases, only the lowest-energy configuration is shown. [b]Flexible SPC model used. [c]Clay–C_{60} Dreiding interaction.

dx.doi.org/10.1021/jp402835v | J. Phys. Chem. A 2013, 117, 6602−6611

whether the molecules approach through the 5- or 6-rings. The differences between the energies of aggregation and adsorption were found to be 0.15 and 0.48 eV using the DFT-D2 and vdW-DF methods, respectively. This suggests that a single C_{60} molecule is thermodynamically more stable when adsorbed on clay surfaces, supporting the view that clay minerals are efficient adsorbents for C_{60}.

The interaction between C_{60} and a single water molecule was also studied (Table 2). In each case, relaxation resulted in the hydrogen atoms being closer to the carbon atoms than oxygen. Water was also found to have no preference for adsorbing onto the 5- or 6-ring (the largest difference was 0.009 eV). The average distances between the oxygen of water (O_W) and the carbon of C_{60} were 3.5 and 3.6 Å with and without vdW interactions, respectively.

The water−pyrophyllite interaction was investigated by Zhang et al.,[61] who performed a full investigation of the performance of CLAYFF compared to DFT-D2. The agreement in the trends of binding energies between the two methods was found to be remarkable, although CLAYFF gave slightly shorter hydrogen bond lengths. We calculated the interaction of the most stable configuration using DFT with and without the inclusion of vdW interactions. In both cases, the water molecule was found to form two H-bonds with the surface, with slightly shorter H_W−O distances of 2.12 and 2.34 Å compared to those reported by Zhang et al.[61] This might be due to the use of slightly different settings for the calculations. DFT without the inclusion of van der Waals corrections predicted the two-H-bond configuration for the water molecule with H-bond lengths of 2.24 and 2.32 Å and an energy of −0.06 eV. Both CLAYFF and PFF reproduced the results from DFT-D2 with energies of −0.21 and −0.16 eV, respectively. The H-bond lengths according to CLAYFF are 2.05 and 2.01 Å, compared to 1.75 and 1.77 Å with PFF.

We then assessed three well-known force fields: CVFF, Dreiding, and Amber. The energies in Table 2 show the same qualitative results as obtained by DFT, and the energy differences with DFT for all of the models are, in our view, within the uncertainties of the van der Waals corrected DFT values. However, on balance, we chose the Dreiding force field in combination with CLAYFF, as this combination gave the energies closest to the dispersion-corrected DFT calculations for both aggregation and adsorption, particularly when compared to DFT-D2. All three force fields gave similar results for the interaction with water, and again, the magnitude of the energy values was well within the uncertainty of the ab initio results. Thus, for brevity, we report primarily the results from the MD simulations using CLAYFF/Dreiding. This is followed by a comparison of PFF/CVFF for water but with C_{60} interactions as in the CLAYFF/Dreiding approach to assess the sensitivity of the results to the potentials.

3.2. Interface Structure and Diffusion of C_{60} on Pyrophyllite. We initially studied a C_{60} molecule above the pyrophyllite surface under dry and wet conditions to investigate the influence of water on the adsorption of molecular C_{60} and to compare adsorption to the aggregation process, namely, the formation of a dimer. Two properties that provide useful insight into the interactions of water in the different systems are the residence time (t_r) of water molecules at each carbon atom of C_{60} and the coordination number (CN) of each carbon atom in the C_{60} molecule within the first hydration layer (Figure 2).

The residence time provides information on the transport of water around molecular C_{60}, indicating the extent of its binding.

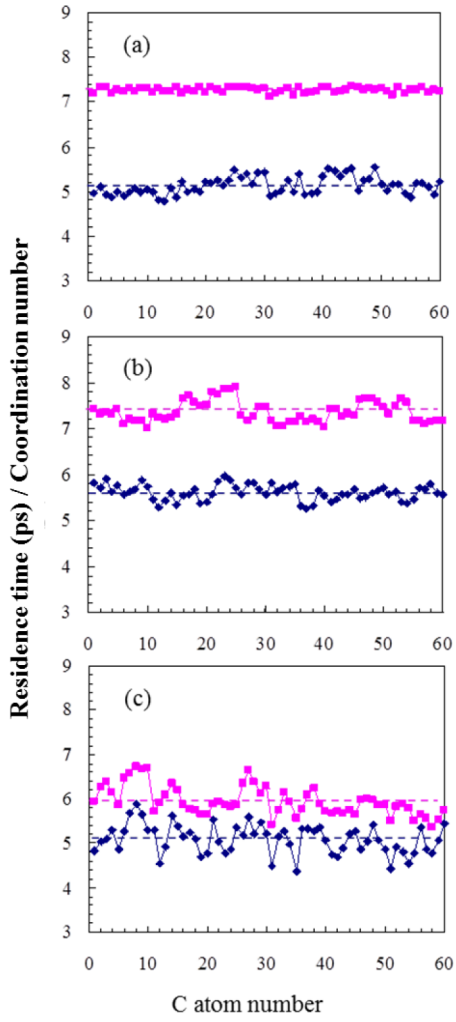

Figure 2. t_r (pink) and CN (blue) values of water molecules around C_{60} in different systems: (a) hydration of a single C_{60} molecule in bulk water, (b) aggregation of two C_{60} molecules in bulk water, and (c) adsorption of a C_{60} molecule on the pyrophyllite surface.

The average t_r values and the average O_W CNs are 5.1 ± 0.2 ps and 7.3 ± 0.1, respectively, for C_{60} in bulk water; 5.6 ± 0.2 ps and 7.4 ± 0.2, respectively, for two aggregated C_{60} molecules in bulk water; and 5.1 ± 0.3 ps and 5.9 ± 0.3, respectively, for C_{60} adsorbed on the surface. Using Amber and TIP4P for water, Hotta et al. reported a value of 4.7 ps for a C_{60} molecule in bulk water, which is in good agreement with our result.[19] The values of t_r according to our calculations are similar within the error, so that the presence of the surface or of another molecule did not significantly affect the mobility of water molecules. However, for C_{60} adsorbed on pyrophyllite, t_r exhibited large fluctuations, which indicates that a number of carbon atoms experienced reduced average contact with the water molecules as C_{60} interacted with the surface. This conclusion is also supported by the smaller average CN value of water molecules on the carbon atoms of C_{60}, which suggests that, on average, 11.5 carbon atoms were not in contact with water as they interacted with the surface. The slightly larger t_r value in the system with aggregated C_{60} molecules compared to those in the other two systems can be attributed to the slower diffusion of clusters compared to molecular C_{60} (0.44×10^{-9} vs 0.52×10^{-9} m^2 s^{-1}). In general, the t_r value of the water oxygen atom (O_W) was found to be small (less than 6 ps) compared to the length

dx.doi.org/10.1021/jp402835v | J. Phys. Chem. A 2013, 117, 6602−6611

of the simulation runs (2 ns), which suggests that the system was well-converged.

Figure 3 shows the time-average image (yellow) of the center of mass of C_{60} displayed every 0.5 ps, illustrating the extent of

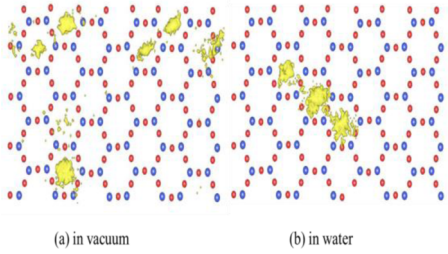

Figure 3. Top views of the time-average images of the center of mass of C_{60} (yellow) calculated every 0.5 ps at 300 K in (a) a vacuum and (b) water on the pyrophyllite surface. O, red; Si, blue.

movement over 2 ns in both a vacuum (Figure 3a) and water (Figure 3b). The most favorable adsorption site is the ditrigonal cavity of the surface. The C_{60} self-diffusion coefficients were calculated from its center of mass on the surface as 5.4×10^{-9} m^2 s^{-1} in a vacuum and 0.3×10^{-9} m^2 s^{-1} in water. The diffusion coefficient of molecular C_{60} was reduced by the presence of water molecules, as expected because of the constraining effect of the solvent H-bonding network.

The side views of the time-average images of O_W and C_{60} on the pyrophyllite surface over 2 ns are shown in Figure 4. The

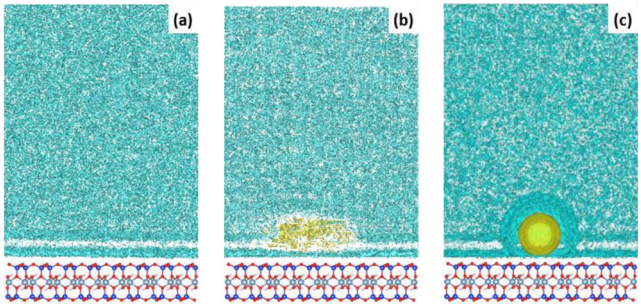

Figure 4. Side views of the time-average images of water (blue) and C_{60} (yellow) for the system with (a) only the water solvent, (b) water and C_{60}, and (c) water and fixed C_{60}. O, red; Si, blue; Al, light blue; H, white.

water density exhibits structure and the formation of two hydration layers on the clay surface, both in the absence (Figure 4a) and in the presence (Figure 4b,c) of the C_{60} molecule. Similar results were reported in previous studies of the hydration of clay mineral surfaces.[62] Disruption of the water layers was seen after the addition of a C_{60} molecule, as it moved between ditrigonal cavities (Figure 4b); the molecule density appears smeared because it was in motion. When the center of mass of C_{60} was fixed (Figure 4c) in the optimum adsorption site, the solvent showed significant structuring around C_{60}, indicating that the molecule markedly impacted the water structure. Similar findings were shown in previous studies.[14,15]

The normalized z-density profiles of O_W and C_{60} carbon atoms are presented in Figure 5. Three peaks were found in the z-density profile of O_W when the C_{60} was present. The first two peaks correspond to the two hydration layers above the surface (Figure 5a). When C_{60} was adsorbed, the first hydration peak shifted closer to the pyrophyllite surface, from 3.0 to 2.8 Å;

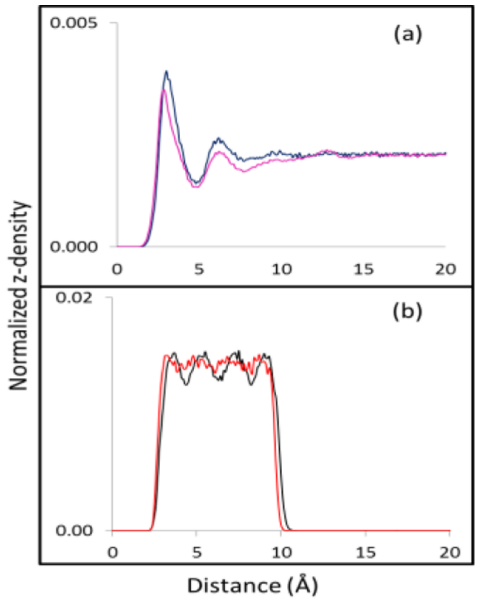

Figure 5. Normalized z-density profiles of (a) O_W and (b) C_{60} carbon atoms on the pyrophyllite surface at 300 K. The distance from the pyrophyllite surface (at $z = 0$) is defined as the time-average position of all surface oxygen atoms. In panel (a), pink and blue lines represent the hydrated systems with and without C_{60}, respectively. In panel (b), red and black lines represent the molecule in a vacuum and in water, respectively.

thus, C_{60} has the effect of "pushing" water molecules closer to the surface as it tumbles between the ditrigonal cavities. The curious third peak at 12.8 Å, which appears a little farther from the distance where the z-density profile of carbon atoms of C_{60} ends (Figure 5b), corresponds to the C_{60} hydration shell. Beyond this peak, the water density converged to the bulk value. The normalized z-density profile of C_{60} carbon atoms (Figure 5b) was smooth in a vacuum and showed small peaks when immersed in water. This implies that, in a vacuum, the molecule tumbles freely whereas, in water, it spends marginally more time spinning, thus giving rise to the peaks.

The radial distribution function (RDF) is another method of viewing the presence of hydration shells and provides complementary information to that obtained from the z-density profile. The RDF of O_W–C_{60} (from its center of mass) and the coordination numbers (CNs) of water around the C_{60} molecule when immersed in bulk water and adsorbed on the hydrated pyrophyllite surface are shown in Figure 6. From the atomistic point of view, the hydration shell comes from the rearrangement of water and H-bonding between water molecules around the C_{60} molecule. The density of the hydration shell is unknown and still debated in the literature from both experimental and computational points of view.[13−22] The first peak of the RDFs, which represents the position of the hydration shell, was found to have its maximum and minimum at approximately 6.9 and 8.4 Å, respectively, in both systems. This suggests that the average O_W–C_{60} distance is 3.5 Å, which is in good agreement with the results of previous studies[14,17] and with our vdW-corrected ab initio calculations, which gave O_W–C_{60} distances of approximately 3.5−3.6 Å.

The calculated O_W coordination numbers for the C_{60} molecule (from its center of mass) corresponding to the first hydration shell are 67 and 54 for C_{60} in bulk water and adsorbed on the pyrophyllite surface, respectively, which

dx.doi.org/10.1021/jp402835v | J. Phys. Chem. A 2013, 117, 6602−6611

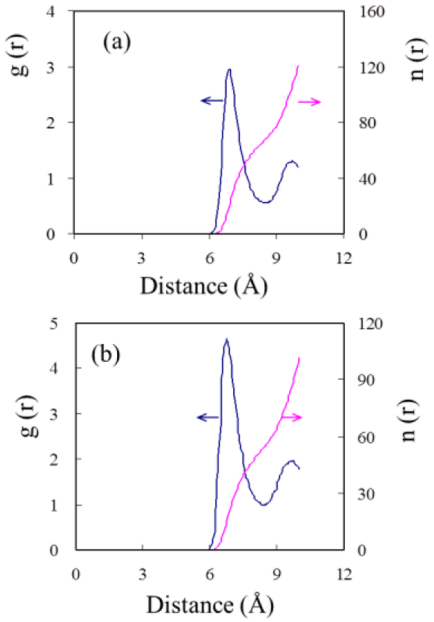

Figure 6. RDFs of O_W−C_{60} (blue line) and CNs of water around C_{60} (pink line) for (a) C_{60} in bulk water and (b) C_{60} adsorbed on a hydrated pyrophyllite surface.

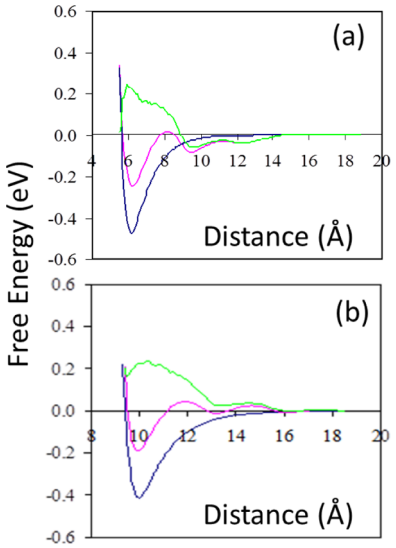

Figure 7. PMF profiles of (a) the adsorption of C_{60} on the pyrophyllite surface and (b) the aggregation of two C_{60} molecules. The distance of separation is defined in panel (a) by the distance between the center of mass of C_{60} and the surface oxygens of the pyrophyllite surface and in panel (b) by the distance between the centers of mass of the two C_{60} molecules. The blue and pink lines represent vacuum and water systems, respectively. The green line is the solvent-induced effect for both the aggregation and adsorption processes.

supports the disruption of the hydration sphere of C_{60} by the surface. Maciel et al.[17] reported CNs between 61 and 66 for C_{60} immersed in bulk water, whereas Li et al.[15] found an average CN of 57 water molecules, depending on the force field used for C_{60}. The small difference between our results and those of Maciel et al.[17] might be the result of our use of the flexible SPC model[27] whereas they used the rigid SPC model for water. Ab initio techniques have also been employed to simulate C_{60}−nH_2O complexes.[22] The water molecules were found to be in straddling positions to achieve the optimization of the coverage. The study included only complexes up to a maximum CN of 60 water molecules in one layer of water. However, by including entropic effects, as in our molecular dynamics, the H-bond network might be more disrupted, so that the water cage around C_{60} can accommodate a greater number of molecules.

3.3. Free Energy Simulations. One key challenge to enable simulations to help and complement experiments is the accurate calculation of the free energies of adsorption and aggregation of molecular C_{60}, as these values can provide distribution coefficients and, hence, the ratio between adsorbed and aggregated C_{60}.

The free energy changes in a vacuum and in water at 300 K for the adsorption of C_{60} on pyrophyllite and for the aggregation of two C_{60} molecules are shown in Figure 7 as functions of the distance from the surface and the center of mass of the molecule, respectively. The errors in precision, by comparison of independent simulations, were found to be small and were less than 0.005 eV for the adsorption and aggregation free energies.

The free energy profile for C_{60} adsorbing in a vacuum on pyrophyllite (Figure 7a) shows only a single minimum at 6.3 Å with an energy of −0.47 (±0.9%) eV, whereas in water, two minima were found. The global minimum was also found at 6.3 Å, but with an adsorption energy of −0.25 (±2.6%) eV. When a molecule adsorbed in the global minimum, it formed an inner-sphere complex, that is, it was in direct contact with the surface. Similarly, the free energy profile for the aggregation of two C_{60} molecules in water (Figure 7b) was found to have a global minimum at 10 Å with an energy of −0.19 (±2.9%) eV, which is 0.22 eV less negative than the value in a vacuum [−0.41 (±1.7%) eV]. The calculated separation distance between C_{60} molecules is, therefore, on average, 3.4 Å, which agrees well with the DFT average value of 3.5 Å. The decrease in the energy upon inclusion of the solvent (0.22 eV) in the case of C_{60} aggregation was previously attributed to the high molecular density of C_{60}, which, in turn, results in a strong van der Waals interaction with water molecules.[14,15] The energy at the minimum (9.8 Å) agrees well with the previously reported value of approximately −0.23 eV from Hotta et al.[19] The simulations suggest that water molecules form a hydration shell around C_{60} that makes the aggregation of C_{60} molecules less favorable in water than in a vacuum, and obviously, a similar effect was calculated for the adsorption of molecular C_{60} on pyrophyllite surfaces. The free energy of adsorption on pyrophyllite was always found to be more negative than the free energy of aggregation, and therefore, when a C_{60} molecule is present in the environment, it will thermodynamically prefer to be retained on the surface of pyrophyllite (and other clay minerals with similar structures) rather than aggregated in clusters. Another feature of the free energy calculations (Figure 7) is that the free energy profiles also show energy barriers that need to be overcome by molecular C_{60} before approaching the surface or another molecule. Interestingly, the energy barrier for the aggregation [0.04 (±1.6%) eV] was found to be larger than that for adsorption [0.02 (±3.5%) eV], indicating that the rate of C_{60} adsorption on the pyrophyllite surface will be greater than the rate of aggregation. Finally, the free energy profiles show a local minimum beyond the energy barrier in water, corresponding to an outer-sphere complex. The free energies were found to be −0.1 (±0.7%) eV for adsorption and −0.01 (±6.3%) eV for aggregation.

dx.doi.org/10.1021/jp402835v | J. Phys. Chem. A 2013, 117, 6602−6611

These free energies can be used to estimate the ratio of molecular C_{60} adsorbed on the surface to that aggregated in clusters as K_{ads}/K_{agg}, as $K_{ads} = \exp(-\Delta G_{ads}/RT)$ and $K_{agg} = \exp(-\Delta G_{agg}/RT)$ are the adsorption and aggregation constants, respectively. We calculated $K_{ads}/K_{agg} \approx 10$ at 300 K, suggesting that, when clay is present, C_{60} will preferably adsorb.

Finally, we calculated the water-induced interaction free energy, which is the difference between the free energy of interaction between two species (either two C_{60} molecules or the C_{60} particle and the surface) in a vacuum and in water and, thereby, evaluated the contribution of water molecules to the aggregation and adsorption processes. This difference includes the water−particle and water−surface interactions, but there is controversy over whether water−water interactions impact the free energy of interaction between particles. Our results suggest that they do and, hence, that the water-induced interaction is a many-body effect, as the interactions between the particle and the surface are dependent on the solvent−solvent interaction.

The water-induced interaction free energy (Figure 7b) was found to always make a positive (i.e., unfavorable) contribution to the aggregation process, as it requires work to disrupt the hydration layers of the C_{60} molecules, which is consistent with the results of previous studies by Li et al.[14,15] It is worth noting that, below the energy barrier up to contact distance, we calculated a positive water-induced effect even though there was no solvent between the two carbon nanoparticles. This can be attributed to the force exerted by the water molecules as they attempt to fill the vacuum between the two C_{60} molecules. At very close distances, the interaction of water molecules with each other is more significant than the direct water−C_{60} interaction, which, at short C_{60}−C_{60} distances, is invariant, as shown previously by Hotta et al.[19] The fact that the water-induced interaction is a many-body effect is the reason our results might appear in contrast to those of Hotta et al.,[19] who also reported the solvent-induced contribution to the aggregation of two C_{60} molecules to be positive but slowly decreasing for distances below the energy barrier. However, their definition included only the C_{60}−water contribution and not the water−water contribution.

In contrast, the water-induced interaction free energy of adsorption was found to be negative and, hence, favorable for C_{60} adsorption at the surface from 9 to 14 Å (Figure 7a). This favorable contribution acts to attract the molecule toward the surface and is due to the interaction between the second surface hydration layer and the hydration layer of the C_{60} molecule. This finding supports the possibility that C_{60} molecules undergo outer-sphere adsorption, which occurs at the local energy minimum at 9.6 Å. As the C_{60} molecule approaches the surface and its hydration layer crashes into the first hydration layer of the surface, this gives rise to a positive contribution similar to that seen in aggregation, and inner-sphere adsorption at the global minimum at 6.3 Å can occur (only once the energy barrier at 8.2 Å is overcome). At short distances between C_{60} and the surface, the predominant terms in the water-induced contribution are the water−water and water−surface interactions.

We also correlated the normalized density profile of water and the adsorption free energy profile of the center of mass of C_{60} (Figure 8) with the H-bonding network to obtain a better understanding of the influence of the solvent-induced interaction on the (outer and inner) adsorption of C_{60} on the pyrophyllite surface. Specifically, we redrew the free energy profile with the x axis corresponding to the carbon atom closest

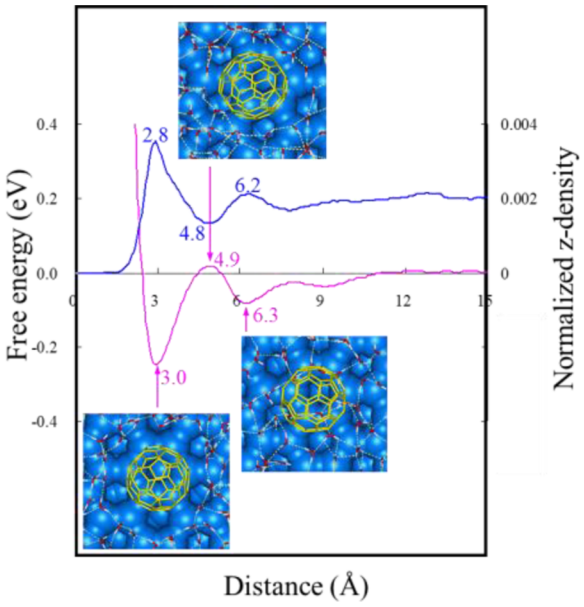

Figure 8. Normalized z-density profile of water (blue line) and PMF adsorption profile (pink line). Note that the PMF profile is shifted by the half-width of the C_{60} molecule according to the z-density profile of carbon atoms of C_{60} (3.3 Å). The top views of the adsorbed C_{60} on the surface show the water molecules and H-bonds (dashed lines) around C_{60} at the global energy minimum (3.0 Å), energy barrier (4.9 Å), and local energy minimum (6.3 Å).

to the clay surface (Figure 8). Thus, the global minimum, energy barrier, and local minimum appeared when the closest carbon atoms were 3.0, 4.9, and 6.3 Å, respectively, from the surface. These free energy minima correlate well with the maxima in the water density. Visual inspection of the configurations recorded during the MD runs (see inset snapshot in Figure 8) shows a very clear pattern. At the local energy minimum (6.3 Å), the C_{60} molecule is within the second hydration layer of the siloxane surface, and water molecules show an extensive H-bonding network below the molecule, suggesting that C_{60} forms outer-sphere complex. As the molecule approaches the surface, it needs to compete with the adsorbed water molecules and has to break the H-bonding network, thus giving rise to the energy barrier at 4.9 Å. Indeed, the snapshot in Figure 8 shows that the water layer closest to the surface becomes disrupted as the water molecules rearrange around the C_{60} molecule and create a cavity to accommodate it. When the barrier is overcome, the interaction between the molecule and the surface becomes dominant. The size of the cavity increases to fully accommodate the C_{60} molecule as it continues to approach the surface. Locally, the first hydration layer is broken, and the H-bonding network is completely disrupted as the molecule reaches the adsorption equilibrium position (global energy minimum at 3.0 Å), which is the ditrigonal cavity of the siloxane surface. This is clearly the more stable inner-sphere adsorption complex.

3.4. Impact of the Surface Properties on the Adsorption Energy. One important consideration when using potential-based techniques is the sensitivity of the results to the details of the force fields. For example, PFF reproduces the surface tension of pyrophyllite quantitatively, whereas CLAYFF overestimates the value.[24,28] We therefore tested the importance by comparing the free energy calculation results of the two independently derived models. We retained the

dx.doi.org/10.1021/jp402835v | J. Phys. Chem. A 2013, 117, 6602−6611

Dreiding model for intermolecular forces for the C_{60} molecule as in the previous PMF calculations based on CLAYFF.

The structural features of the clay−water interface simulated using PFF are very similar to those obtained the CLAYFF simulations. On average, the oxygen of water (O_W) was at 2.9 Å, and the center of mass of the carbon nanoparticle adsorbed 6.1 Å above the surface layer of oxygen ions. As a reminder, the O_W and C_{60} center of mass were found to adsorb, on average, 3.0 and 6.1 Å from the surface oxygen ions using CLAYFF.

The free energy changes in a vacuum and in water at 300 K using PFF for the adsorption of C_{60} on pyrophyllite are shown in Figure 9 as functions of the distance from the surface.

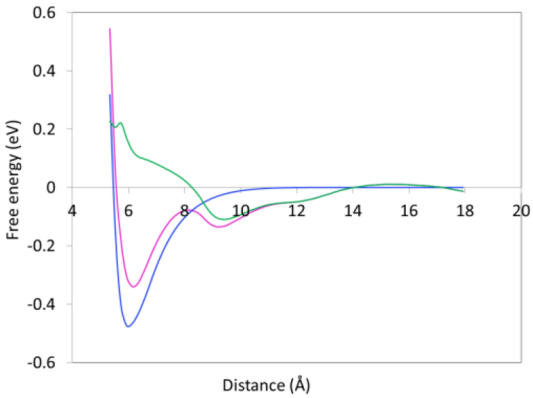

Figure 9. PMF profiles of the adsorption of C_{60} on the pyrophyllite surface. The distance of separation is defined by the distance between the center of mass of C_{60} and the surface oxygens of the pyrophyllite surface. The blue and pink lines represent vacuum and water systems, respectively. The green line shows the solvent-induced effect for the adsorption processes.

The PMF for the aggregation of two C_{60} molecules in water at 300 K was also recalculated, as the water model associated with PFF is different and not indistinguishable from that calculated using CLAYFF. Similarities with the free energies calculated using CLAYFF (Figure 7a) are apparent. As before, only one minimum was obtained for C_{60} in a vacuum adsorbed on pyrophyllite at 6.0 Å with an energy of −0.47 (±7.1%) eV, whereas, in water, a global minimum was found at 6.1 Å with an adsorption energy of −0.33 (±1.6%) eV when the C_{60} adsorbed directly onto the surface forming an inner-sphere complex and a local minimum was found at 9.1 Å with an adsorption energy of −0.13 (±3.0%) when the outer-sphere complex was formed.

Again, the free energy of adsorption on pyrophyllite was always found to be more negative than the free energy of aggregation, leading to the same conclusion. A single C_{60} molecule has a thermodynamic preference to be retained on the pyrophyllite surfaces rather than aggregated in clusters.

The only difference observed for the PFF model was that the energy barrier from the outer-sphere to the inner-sphere complex was lower (0.06 eV) than that for CLAYFF (0.1 eV), although there was still an energetic cost. Thus, the energy barrier for aggregation is still present, and therefore, using the PFF model, the adsorption seems to be barrierless, supporting the original idea that clay minerals can adsorb single C_{60} molecules before aggregation occurs.

The water-induced effect shows the same features as for the CLAYFF calculations, again leading to the same conclusions. There is a favorable driving force for the carbon particles to adsorb above the energy barrier.

4. CONCLUSIONS

In summary, we have shown that simulations can be used to complement experimental data and predict data that otherwise would be difficult to obtain experimentally. In addition, we showed that computer simulations can provide useful atomistic insight into the interaction of C_{60} with clay surfaces in aqueous solution, although, clearly, the techniques described here can be applied to any nanoparticle on any mineral surface.

The results for the adsorption of molecular C_{60} on pyrophyllite and aggregation of C_{60} show the importance of dispersion corrections in DFT calculations. The energies were calculated to be unfavorable when the van der Waals interactions were neglected, which is clearly incorrect. In the MD simulations, three force fields for the C_{60}−surface, C_{60}−C_{60}, and C_{60}−H_2O were tested against each other and against ab initio results. All were adequate, but the combination of the Dreiding and CLAYFF force fields proved to be the most reasonable choice. The PFF model was used as a comparison, as it describes quantitatively the surface properties of pyrophyllite. All simulations indicated that the ditrigonal cavity on the siloxane surface of pyrophyllite is the main adsorption site for molecular C_{60}. Our time-average images show that C_{60} is surrounded by a hydration shell that is largely maintained even when adsorbed on pyrophyllite and that the water is structured above the surface. Molecular C_{60} can adsorb as outer-sphere and inner-sphere complexes. In the former, the second hydration layer of the surface is disrupted, with the molecule floating on top of the first hydration layer, whereas in the latter, the molecule is directly adsorbed on the surface within the first hydration layer above the surface.

The free energy profiles show that the C_{60} molecule is more likely to be adsorbed on the pyrophyllite surface than aggregated in clusters both in a vacuum and in water, as also supported by dispersion-corrected DFT energy calculations. The results suggest that, in aqueous environments, the concentration of adsorbed C_{60} can be up to 1 order of magnitude larger than the concentration of aggregated C_{60}. The simulations predict that, in an aqueous environment, the energy required to disrupt the hydration shell of the pyrophyllite surface and/or of the C_{60} molecule accounts for the presence of the energy barriers. In addition, we showed that the adsorption of molecular C_{60} in an inner-sphere complex is thermodynamically more stable than that in an outer-sphere complex.

In conclusion, we have shown that hydrophobic clay mineral surfaces can be active sites for environmental remediation of molecular C_{60}, which will strongly influence its transport and fate in the environment. We infer that the effects calculated herein are likely to be reproduced when other carbon-based nanoparticles adsorb at mineral clay surfaces, and hence, we predict that these are generic effects, which, in turn, further suggests that these materials will provide a sustainable and inexpensive method of trapping carbon-based pollutants, as clay minerals are ubiquitous in the environment.

AUTHOR INFORMATION

Corresponding Author

*E-mail: s.c.parker@bath.ac.uk.

Notes

The authors declare no competing financial interest.

dx.doi.org/10.1021/jp402835v | J. Phys. Chem. A 2013, 117, 6602−6611

■ ACKNOWLEDGMENTS

This work was financially supported by the "One Hundred Talents Program" of the Chinese Academy of Sciences (KZZD-EW-TZ-10), a grant from the Royal Society BP Amoco Research Fellowship (RC-CH1054), and grants from the National Natural Science Foundation of China (20907038, 21177104). This is Contribution No. IS-1706 from GIGCAS. The University of Bath acknowledges EPSRC for funding (EP/H005838/1). Computations were run on HPC Aquila at the University of Bath and HECToR facilities through the Materials Chemistry Consortium.

■ REFERENCES

(1) Gogotsi, Y. *Nanomaterials Handbook*; Taylor & Francis: London, 2006.
(2) Dennler, G.; Scharber, M. C.; Brabec, C. J. Polymer−Fullerene Bulk Heterojunction Solar Cells. *Adv. Mater.* **2009**, *21*, 1323−1338.
(3) Tremblay, J. F. Mitsubishi Chemical Aims at Breakthrough. *Chem. Eng. News* **2002**, *80*, 16−17.
(4) Sayes, C. M.; Fortner, J. D.; Guo, W.; Lyon, D.; Boyd, A. M.; Ausman, K. D.; Tao, Y. J.; Sitharaman, B.; Wilson, L. J.; Hughes, J. B.; West, J. L.; Colvin, V. L. The Differential Cytotoxicity of Water-Soluble Fullerenes. *Nano Lett.* **2004**, *4*, 1881−1887.
(5) Song, M.; Yuan, S.; Yin, J.; Wang, X.; Meng, Z.; Wang, H.; Jiang, G. Size-Dependent Toxicity of Nano-C_{60} Aggregates: More Sensitive Indication by Apoptosis-Related Bax Translocation in Cultured Human Cells. *Environ. Sci. Technol.* **2012**, *46*, 3457−3464.
(6) Hou, W. C.; Moghadam, B. Y.; Westerhoff, P.; Posner, J. D. Distribution of Fullerene Nanomaterials between Water and Model Biological Membranes. *Langmuir* **2011**, *27*, 11899−11905.
(7) Qiao, R.; Roberts, A. P.; Mount, A. S.; Klaine, S. J.; Ke, P. C. Translocation of C_{60} and Its Derivatives across a Lipid Bilayer. *Nano Lett.* **2007**, *7*, 614−619.
(8) Chen, C. Y.; Jafvert, C. T. Sorption of Buckminsterfullerene (C_{60}) to Saturated Soils. *Environ. Sci. Technol.* **2009**, *43*, 7370−7375.
(9) Li, Q.; Xie, B.; Hwang, Y. K.; Xu, Y. Kinetics of C_{60} Fullerene Dispersion in Water Enhanced by Natural Organic Matter and Sunlight. *Environ. Sci. Technol.* **2009**, *43*, 3574−3579.
(10) Li, Y.; Wang, Y.; Pennell, K. D.; Abriola, L. M. Investigation of the Transport and Deposition of Fullerene (C_{60}) Nanoparticles in Quartz Sands under Varying Flow Conditions. *Environ. Sci. Technol.* **2008**, *42*, 7174−7180.
(11) Fortner, J. D.; Solenthaler, C.; Hughes, J. B.; Puzrin, A. M.; Plotze, M. Interactions of Clay Minerals and a Layered Double Hydroxide with Water Stable, Nano Scale Fullerene Aggregates. *Appl. Clay Sci.* **2012**, *55*, 36−43.
(12) Jafvert, C. T.; Kulkarni, P. P. Buckminsterfullerene's (C_{60}) Octanol−Water Partition Coefficient (K_{ow}) and Aqueous Solubility. *Environ. Sci. Technol.* **2008**, *42*, 5945−5950.
(13) Labille, J.; Masion, A.; Ziarelli, F.; Rose, J.; Brant, J.; Villieras, F.; Pelletier, M.; Borschneck, D.; Wiesner, M. R.; Bottero, J. Y. Hydration and Dispersion of C_{60} in Aqueous Systems: The Nature of Water−Fullerene Interactions. *Langmuir* **2009**, *25*, 11232−11235.
(14) Li, L.; Bedrov, D.; Smith, G. D. A Molecular-Dynamics Simulation Study of Solvent-Induced Repulsion between C_{60} Fullerenes in Water. *J. Chem. Phys.* **2005**, *123*, 204504-1−204504-7.
(15) Li, L.; Bedrov, D.; Smith, G. D. Water-Induced Interactions between Carbon Nanoparticles. *J. Phys. Chem. B* **2006**, *110*, 10509−10513.
(16) Choudhury, N. Dynamics of Water in Solvation Shells and Intersolute Regions of C_{60}: A Molecular Dynamics Simulation Study. *J. Phys. Chem. C* **2007**, *111*, 2565−2572.
(17) Maciel, C.; Fileti, E. E.; Rivelino, R. Note on the Free Energy of Transfer of Fullerene C_{60} Simulated by Using Classical Potentials. *J. Phys. Chem. B* **2009**, *113*, 7045−7048.
(18) Kim, H.; Bedrov, D.; Smith, G. D. Molecular Dynamics Simulation Study of the Influence of Cluster Geometry on Formation of C_{60} Fullerene Clusters in Aqueous Solution. *J. Chem. Theory Comput.* **2008**, *4*, 335−340.
(19) Hotta, T.; Kimura, A.; Sasai, M. Fluctuating Hydration Structure around Nanometer-Size Hydrophobic Solutes. I. Caging and Drying around C_{60} and $C_{60}H_{60}$ Spheres. *J. Phys. Chem. B* **2005**, *109*, 18600−18608.
(20) Choudhury, N. A Molecular Dynamics Simulation Study of Buckyballs in Water: Atomistic Versus Coarse-Grained Models of C_{60}. *J. Chem. Phys.* **2006**, *125*, 034502-1−034502-7.
(21) Hernandez-Rojas, J.; Breton, J.; Gomez Llorente, J. M.; Wales, D. J. Global Potential Energy Minima of $C_{60}(H_2O)_n$ Clusters. *J. Phys. Chem. B* **2006**, *110*, 13357−13362.
(22) Ludwig, R.; Appelhagen, A. Calculation of Clathrate-like Water Clusters Including H_2O-Buckminsterfullerene. *Angew. Chem., Int. Ed.* **2005**, *44*, 811−815.
(23) Cygan, R. T.; Greathouse, J. A.; Heinz, H.; Kalinichev, A. G. Molecular Models and Simulations of Layered Materials. *J. Mater. Chem.* **2009**, *19*, 2470−2481.
(24) Heinz, H. Clay Minerals for Nanocomposites and Biotechnology: Surface Modification, Dynamics and Responses to Stimuli. *Clay Minerals* **2012**, *47*, 205−230.
(25) Boek, E. S.; Coveney, P. V.; Skipper, N. T. Monte Carlo Molecular Modeling Studies of Hydrated Li-, Na-, and K-Smectites: Understanding the Role of Potassium as a Clay Swelling Inhibitor. *J. Am. Chem. Soc.* **1995**, *117*, 12608−12617.
(26) Skipper, N. T.; Chang, F. C.; Sposito, G. Monte Carlo Simulations of Interlayer Molecular Structure in Swelling Clay Minerals. 1. Methodology. *Clays Clay Miner.* **1995**, *43*, 285−293.
(27) Cygan, R. T.; Liang, J. J.; Kalinichev, A. G. Molecular Models of Hydroxide, Oxyhydroxide, and Clay Phases and the Development of a General Force Field. *J. Phys. Chem. B* **2004**, *108*, 1255−1266.
(28) Heinz, H.; Koerner, H.; Anderson, K. L.; Vaia, R. A.; Farmer, B. L. Force Field for Mica-Type Silicates and Dynamics of Octadecylammonium Chains Grafted to Montmorillonite. *Chem. Mater.* **2005**, *17*, 5658−5669.
(29) Hinchliffe, A. *Molecular Modelling for Beginners*, 2nd ed.; John Wiley & Sons: New York, 2008.
(30) Bergaya, F.; Theng, B. K. G.; Lagaly, G. *Handbook of Clay Science*; Elsevier: Amsterdam, 2006.
(31) Lee, J. H.; Guggenheim, S. Single Crystal X-ray Refinement of Pyrophyllite-1Tc. *Am. Mineral.* **1981**, *66*, 350−357.
(32) Gren, W.; Parker, S. C.; Slater, B.; Lewis, D. W. Structure of Zeolite A (LTA) Surfaces and the Zeolite A/Water Interface. *J. Phys. Chem. C* **2010**, *114*, 9739−9747.
(33) Spagnoli, D.; Allen, J. P.; Parker, S. C. The Structure and Dynamics of Hydrated and Hydroxylated Magnesium Oxide Nanoparticles. *Langmuir* **2011**, *27*, 1821−1829.
(34) Molinari, M.; Parker, S. C.; Sayle, D. C.; Islam, M. S. Water Adsorption and Its Effect on the Stability of Low Index Stoichiometric and Reduced Surfaces of Ceria. *J. Phys. Chem. C* **2012**, *116*, 7073−7082.
(35) Allen, J. P.; Marmier, A.; Parker, S. C. Atomistic Simulation of Surface Selectivity on Carbonate Formation at Calcium and Magnesium Oxide Surfaces. *J. Phys. Chem. C* **2012**, *116*, 13240−13251.
(36) Sposito, G.; Skipper, N. T.; Sutton, R.; Park, S.; Soper, A. K.; Greathouse, J. A. Surface Geochemistry of Clay Minerals. *Proc. Natl. Acad. Sci. U.S.A.* **1999**, *96*, 3358−3364.
(37) Lindgreen, H.; Garnaes, J.; Hansen, P. L.; Besenbacher, F.; Laegsgaard, E.; Stensgaard, I.; Gould, S. A. C.; Hansma, P. K. Ultrafine Particles of North Sea Illite/Smectite Clay Minerals Investigated by STM and AFM. *Am. Mineral.* **1991**, *76*, 1218−1222.
(38) Kresse, G.; Hafner, J. *Ab initio* Molecular-Dynamics Simulation of the Liquid-Metal−Amorphous-Semiconductor Transition in Germanium. *Phys. Rev. B* **1994**, *49*, 14251−14269.
(39) Kresse, G.; Furthmuller, J. Efficient Iterative Schemes for *ab Initio* Total Energy Calculations Using a Plane-Wave Basis Set. *Phys. Rev. B* **1996**, *54*, 11169−11186.
(40) Blöchl, P. E. Projector Augmented-Wave Method. *Phys. Rev. B* **1994**, *50*, 17953−17979.

(41) Kresse, G.; Joubert, D. From Ultrasoft Pseudopotentials to the Projector Augmented-Wave Method. *Phys. Rev. B* **1999**, *59*, 1758−1775.
(42) Perdew, J. P.; Burke, K.; Ernzerhof, M. Generalized Gradient Approximation Made Simple. *Phys. Rev. Lett.* **1996**, *77*, 3865−3868.
(43) Dobson, J. F.; McLennan, K.; Rubio, A.; Wang, J.; Gould, T.; Le, H. M.; Dinte, B. P. Prediction of Dispersion Forces: Is There a Problem? *Aust. J. Chem.* **2001**, *54*, 513−527.
(44) Wu, Q.; Yang, W. Empirical Correction to Density Functional Theory for van der Waals Interactions. *J. Chem. Phys.* **2002**, *116*, 515−524.
(45) Grimme, S. Semiempirical GGA-type Density Functional Constructed with a Long-Range Dispersion Correction. *J. Comput. Chem.* **2006**, *27*, 1787−1799.
(46) Klimeš, J.; Bowler, D. R.; Michaelides, A. Van der Waals Density Functionals Applied to Solids. *Phys. Rev. B* **2011**, *83*, 195131-1−195131-13.
(47) Oliver, P. M.; Parker, S. C.; Mackrodt, W. C. Computer Simulation of the Crystal Morphology of NiO. *Modell. Simul. Mater. Sci. Eng.* **1993**, *1*, 755−760.
(48) Smith, W.; Forester, T. R. DL_POLY_2.0: A General-Purpose Parallel Molecular Dynamics Simulation Package. *J. Mol. Graphics* **1996**, *14*, 136−141.
(49) Zhu, R.; Chen, W.; Shapley, T. V.; Molinari, M.; Ge, F.; Parker, S. C. Sorptive Characteristics of Crganomontmorillonite toward Organic Compounds: A Combined LFERs and Molecular Dynamics Simulation Study. *Environ. Sci. Technol.* **2011**, *45*, 6504−6510.
(50) Liu, X.; Lu, X.; Wang, R.; Zhou, H.; Xu, S. Molecular Dynamics Insight into the Cointercalation of Hexadecyltrimethyl-Ammonium and Acetate Ions into Smectites. *Am. Mineral.* **2009**, *94*, 143−150.
(51) Wang, J.; Kalinichev, A. G.; Kirkpatrick, R. J.; Cygan, R. T. Structure, Energetic and Dynamics of Water Adsorbed on the Muscovite (001) Surfaces: A Molecular Dynamics Simulation. *J. Phys. Chem. B* **2005**, *109*, 15893−15905.
(52) Greathouse, J. A.; Cygan, R. T. Water Structure and Aqueous Uranyl(VI) Adsorption Equilibria onto External Surfaces of Beidellite, Montmorillonite, and Pyrophyllite: Results from Molecular Simulations. *Environ. Sci. Technol.* **2006**, *40*, 3865−3871.
(53) Du, H.; Miller, J. D. Adsorption States of Amphipatic Solutes at the Surface of Naturally Hydrophobic Minerals: A Molecular Dynamics Simulation Study. *Langmuir* **2007**, *23*, 11587−11596.
(54) Zeitler, T. R.; Greathouse, J. A.; Cygan, R. T. Effects of Thermodynamic Ensembles and Mineral Surfaces on Interfacial Water Structure. *Phys. Chem. Chem. Phys.* **2012**, *14*, 1728−1734.
(55) Dauber-Osguthorpe, P.; Roberts, V. A.; Osguthorpe, D. J.; Wolff, J.; Genest, M.; Hagler, A. T. Structure and Energetics of Ligand Binding to Proteins: *Escherichia coli* Dihydrofolate Reductase Trimethoprim, a Drug-Receptor System. *Proteins: Struct. Funct. Genet.* **1988**, *4*, 31−47.
(56) Mayo, S. L.; Olafson, B. D.; Goddard, W. A., III. Dreiding: A Generic Force Field for Molecular Simulations. *J. Phys. Chem.* **1990**, *94*, 8897−8909.
(57) Cornell, W. D.; Cieplak, P.; Bayly, C. I.; Gould, I. R.; Merz, K. M., Jr.; Ferguson, D. M.; Spellmeyer, D. C.; Fox, T.; Caldwell, J. W.; Kollman, P. A. A Second Generation Force Field for the Simulation of Proteins, Nucleic Acids, and Organic Molecules. *J. Am. Chem. Soc.* **1995**, *117*, 5179−5197.
(58) Kerisit, S.; Parker, S. C. Free Energy of Adsorption of Water and Metal Ions on the {104} Calcite Surface. *J. Am. Chem. Soc.* **2004**, *126*, 10152−10161.
(59) Kerisit, S.; Cooke, D. J.; Spagnoli, D.; Parker, S. C. Molecular Dynamics Simulations of the Interactions between Water and Inorganic Solids. *J. Mater. Chem.* **2005**, *15*, 1454−1462.
(60) Watson, G. W.; Kelsey, E. T.; de Leeuw, N. H.; Harris, D. J.; Parker, S. C. Atomistic Simulation of Dislocations, Surfaces and Interfaces in MgO. *J. Chem. Soc., Faraday Trans.* **1996**, *92*, 433−438.
(61) Zhang, G.; Al-Saidi, W. A.; Myshakin, E. M.; Jordan, K. D. Dispersion-Corrected Density Functional Theory and Classical Force Field Calculations of Water Loading on a Pyrophyllite (001) Surface. *J. Phys. Chem. C* **2012**, *116*, 17134−17141.
(62) Wang, J.; Kalinichev, A. G.; Kirkpatrick, R. J. Effects of Substrate Structure and Composition on the Structure, Dynamics, and Energetics of Water at Mineral Surfaces: A Molecular Dynamics Modeling Study. *Geochim. Cosmochim. Acta* **2006**, *70*, 562−582.